RSC Advances

PAPER

View Article Online
View Journal | View Issue

Cite this: *RSC Adv.*, 2025, **15**, 14158

Development of sulfonated polystyrene resin-supported tungsten oxide for Pb^{2+} ion sequestration†

Kashmala Khaliq,[a] Mohsin Ali Raza Anjum,[b] Shabnam Shahida,*[a] Ramzan Akhtar,[b] Adil Khan,[b] Munib Ahmad Shafiq,[c] Iqra Rafiq,[d] Muhammad Rehan,[e] Rashid Nazir Qureshi,[c] Sajid Iqbal,*[f] Jong-Il Yun*[f] and Muhammad Saifullah*[b]

A sulfonated polystyrene resin-supported tungsten oxide (SO_3-PSWO) was synthesized and evaluated for its efficiency in removing lead (Pb^{2+}) from aqueous solutions. Morphology, phase purity, structural properties, thermal stability, and elemental composition of SO_3-PSWO, are evaluated using SEM, XRD, FTIR, TGA, and CHNS analyzers. The ICP-OES technique was utilized for quantitative measurements of the Pb^{2+} ions. The influence of key parameters such as pH, adsorbent dose, contact time, metal ion concentration, temperature, and interference of competing ions on Pb^{2+} removal is systematically investigated. Under optimum conditions (pH 3.5–5.5), SO_3-PSWO achieved a maximum Pb^{2+} removal efficiency of 99.7% within one hour and demonstrated an exceptional adsorption capacity of 386 mg g^{-1}, as described by the Langmuir isotherm model. Kinetic analysis revealed a pseudo-second-order mechanism, highlighting chemisorption as the predominant process. Thermodynamic studies indicated an exothermic and spontaneous adsorption behavior. With its easy synthesis, cost-effectiveness, rapid kinetics, high adsorption capacity, and superior efficiency, SO_3-PSWO emerges as a promising material for the remediation of Pb^{2+} contamination in water treatment applications.

Received 12th February 2025
Accepted 17th April 2025

DOI: 10.1039/d5ra01017a

rsc.li/rsc-advances

1. Introduction

The contamination of water with heavy metals such as Pb, Cd, As, Cu, Cr, Ni, Hg, Mn, and Zn poses a significant global environmental challenge due to their detrimental effects on public health and the ecosystem.[1–9] According to the World Health Organization (WHO),[10] over 785 million people worldwide lack access to clean drinking water, with a substantial portion of water sources contaminated by heavy metals. Metal-polluted wastewater must be treated to reduce hazardous substances to permissible levels before being released into the environment.[11]

Among heavy metals, lead (Pb^{2+}) is particularly hazardous and carcinogenic.[12] Prolonged exposure can cause aminoaciduria, glycosuria, renal cancer, liver failure, skeletal abnormalities, neurological impairment, cardiovascular diseases, developmental disorders, and immune system suppression by reducing immunoglobulin-producing cells and inhibiting antibody synthesis.[13–16] Pb^{2+} contamination has increased in recent years, especially in China. In Pakistan, water systems in Balochistan have reported Pb^{2+} concentrations ranging from 0.0010 to 0.063 mg L^{-1}, significantly exceeding the U.S. Environmental Protection Agency (EPA) standard of 0.015 mg L^{-1}. The WHO and EPA set maximum Pb^{2+} levels in drinking water at 10 μg L^{-1} and 15 μg L^{-1}, respectively.[17,18] Whether ingested or inhaled, Pb^{2+} has severe physiological effects, but effective strategies and preventive measures can help mitigate these risks.[16]

Various methods such as ion exchange, chemical precipitation, solvent extraction, and membrane filtration have been used for heavy metal removal, these techniques often face challenges like incomplete contaminant removal, high energy costs, and toxic sludge production.[19–23] Among them, adsorption stands out due to its simplicity, cost-effectiveness, and reusability of adsorbents after treatment.[24–26] Traditional adsorbents, including activated carbon and polymeric ion exchangers, face limitations such as high operational costs,

[a]*Department of Chemistry, University of Poonch Rawalakot, AJK, Pakistan. E-mail: shabnamshahida01@gmail.com*

[b]*Chemistry Division, Pakistan Institute of Nuclear Science and Technology (PINSTECH), Nilore 45650, Islamabad, Pakistan. E-mail: saifi.551@gmail.com*

[c]*Central Analytical Facility Division, Pakistan Institute of Nuclear Science and Technology (PINSTECH), Nilore 45650, Islamabad, Pakistan*

[d]*Department of Chemistry, Government College University Faisalabad (GCUF), Faisalabad, Pakistan*

[e]*Photovoltaic Research Department, Korea Institute of Energy Research, Daejeon, South Korea*

[f]*Department of Nuclear and Quantum Engineering, KAIST, 291 Deahak-ro, Yuseong-gu, Daejeon 34141, Republic of Korea. E-mail: sajid1@kaist.ac.kr; jiyun@kaist.ac.kr*

† Electronic supplementary information (ESI) available. See DOI: https://doi.org/10.1039/d5ra01017a

reduced efficiency when competing ions are present, and limited selectivity.[27] Functionalized polystyrene, particularly sulfonated forms, has shown promise for heavy metal removal due to its ability to develop diverse polymer matrices.[28] Previous studies have incorporated materials like hydrous zirconium oxide and zirconium oxide nanoparticles into polystyrene for effective Pb^{2+} remediation.[9,29] Inorganic nano-oxides and hydroxides, such as ferric oxide, manganese oxide, cerium hydroxide, activated alumina, and zirconium phosphate, have also demonstrated efficiency in heavy metal removal; however, challenges like low adsorption capacity and poor acid resistance persist.[30–36] Tungsten oxide has emerged as a promising material due to its thermal stability, acid resistance, and abundant oxygen vacancies, providing numerous active sites for heavy metal adsorption. These properties make tungsten oxide highly effective for advancing water purification technologies.[31]

Lead (Pb^{2+}) adsorption using tungsten oxide remains limited, underscoring the need for further investigation. Perkins *et al.*[32] demonstrated that commercially available WO_3 nanopowder exhibits high Pb^{2+} sorption efficiency, achieving an adsorption capacity of 324 mg g^{-1} (36%), highlighting its potential for Pb^{2+} remediation. In a subsequent study, Perkins *et al.*[33] reported that nanoporous WO_3 further enhances Pb^{2+} adsorption, achieving a 42.5% sorption capacity. The increased porosity, faster sorption kinetics, and larger surface area contribute to reducing Pb^{2+} concentration to below 0.5 ppb. Additionally, Umejuru *et al.*[34] functionalized coal fly ash with a graphene oxide–tungsten oxide nanorod composite *via* a hydrothermal process, achieving a Pb^{2+} adsorption capacity of 41.51 mg g^{-1}. These studies highlight the potential of tungsten oxide-based materials for effective Pb^{2+} removal, warranting further exploration of their adsorption mechanisms and practical applications.

The inorganic nanoparticles of tungsten oxide tend to agglomerate, significantly decreasing their effectiveness for separation purposes.[35] Separating ultrafine particles from aqueous systems can be an inefficient, expensive, and challenging task.[36] Powder adsorbents coagulate due to strong van der Waals forces, decreasing their accessible surface area and binding sites, making them less suitable for column or fluidized systems due to high pressure drop and separation difficulties.[37,38] To prevent nanoparticle agglomeration and enhance water treatment efficiency, polystyrene divinyl benzene (PS-DVB) is used as a support material for tungsten oxide. Furthermore, the functionalization of PS-DVB with sulfonic acid enhances its removal efficiency for metal ions, and results in rapid adsorption kinetics as it induces additional active sites and improves the dispersion of tungsten oxide. The porous and functionalized PS-DVB ensure uniform distribution of tungsten oxide particles, maximizing active site exposure for effective Pb^{2+} ion removal from aqueous solution.

This study develops a novel adsorbent by incorporating tungsten oxide onto a polystyrene-based support. The synthesis method is simple, low-temperature, and highly efficient. Tungsten oxide is deposited on pristine and sulfonated polystyrene resins, and their Pb^{2+} adsorption performance is compared. The sulfonated polystyrene resin enables higher tungsten oxide loading due to sulfonic acid groups, which enhance Pb^{2+} adsorption capacity. The results demonstrate that tungsten oxide-functionalized sulfonated polystyrene resin exhibits superior removal efficiency and adsorption capacity, making it a highly effective material for Pb^{2+} remediation.

2. Materials and methods

2.1 Materials

Materials used in this study are divinyl benzene (DVB) (Sigma-Aldrich, 85%), styrene (98%), ethanol (C_2H_5OH) (Merck, 99%), cyclohexanone (Merck, 99%), gelatin pyruvate (Merck, 99%), gum arabic (98%), deionized water (DI), benzoyl peroxide (BPO) (Sigma-Aldrich, 98%), tungsten powder (99%), acetic acid (CH_3COOH) (Merck, 99%), hydrogen peroxide (Merck, 35%), lead chloride ($PbCl_2$) (Sigma-Aldrich, 98%), sulphuric acid (Merck, 97.5%), dichloromethane (99%), nitric acid (HNO_3, 65%), and sodium hydroxide (NaOH, 98%). DI water is used for washing and solution preparation.

2.2 Synthesis of polystyrene divinyl benzene resin-supported tungsten oxide

The synthesis of tungsten oxide encapsulated polystyrene divinyl benzene (PS-DVB) beads includes three main steps.

2.2.1 Synthesis of polystyrene divinyl benzene cation exchanger resin. Fig. 1 shows the systematic synthesis of PS-DVB carried out through suspension polymerization, involving two distinct phases: the organic phase and the aqueous phase. To make the aqueous phase, 3 g each of gelatin and gum arabic are mixed in 250 mL of DI water in a beaker under uniform magnetic stirring. The organic phase is prepared by mixing 20 mL of styrene, 2 mL of DVB, 0.05 g of BPO, and 15 mL of cyclohexanone in a separate beaker. Both phases are combined in a reactor, immersed in a water bath at 95 °C. A mechanical stirrer set to 350 rpm mixes the solutions, facilitating the polymerization reaction for 6 hours. The mixture is subsequently filtered, and the residue is thoroughly washed with hot water, acetone, and DI water to remove impurities. The purified PS-DVB is dried overnight at 60 °C, completing its synthesis.

For sulfonation, 10 g of PS-DVB resin is swollen in 50 mL of dichloromethane overnight. Afterward, 50 mL of concentrated sulfuric acid is added to the swollen resin, and the mixture is stirred at 300 rpm and heated to 85 °C for 5 hours to induce sulfonation. The resin is next washed extensively with DI water to eliminate residual acid and impurities, followed by drying at 60 °C overnight.

2.2.2 Synthesis of acetylated peroxotungstic acid. In the second step, 6.5 g of tungsten powder is gradually added to a mixture of 40 mL hydrogen peroxide and 4 mL DI water while maintaining a low temperature with an ice bath due to the exothermic reaction as illustrated in Fig. 2. After 4 hours, the mixture is brought to room temperature and shaken on an orbital shaker at 250 rpm for 24 hours, during which it turns transparent yellow.

The solution is centrifuged for 2 minutes to separate the tungsten powder. The supernatant is combined with 40 mL of acetic acid and heated at 55 °C for 3 hours, forming a milky

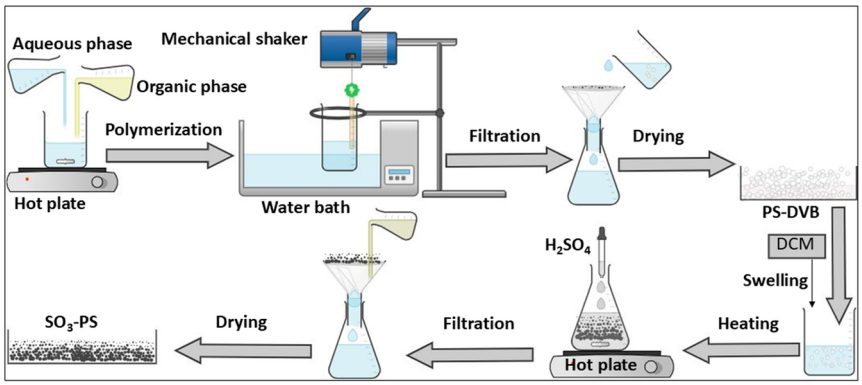

Fig. 1 Schematic illustration of the synthesis process of polystyrene and sulfonated polystyrene resin.

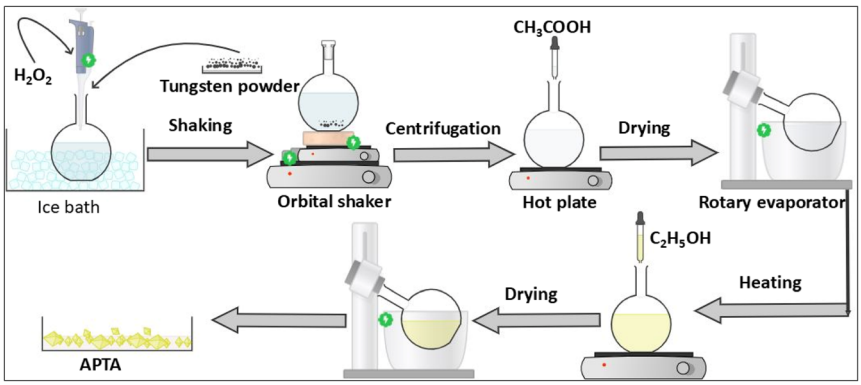

Fig. 2 Schematic illustrations of the synthesis process of APTA.

solution. Solvent removal *via* rotary evaporation yields a white powder, which is dissolved in 50 mL of ethanol and reheated at 55 °C for 3 hours, producing a yellow solution. Finally, acetylated peroxotungstic acid (APTA) is obtained as a yellow powder using a rotary evaporator.

2.2.3 Synthesis of polystyrene- and sulfonated polystyrene resin-supported tungsten oxide. In the 3rd step (Fig. 3), a total of 2.5 g of pristine polystyrene resin and 2.5 g of APTA are added to a flask with 30 mL of ethanol. To ensure complete interaction between polystyrene resin and APTA, the mixture is shaken on an orbital shaker for around 4 h. Afterwards, to aid in the conversion of APTA to tungsten oxide, the solid portion is carefully dried in an oven at 100 °C for 15 hours. The same procedure is used for loading tungsten oxide on sulfonated polystyrene resin. Fig. 3 explains the synthesis process of polystyrene- and sulfonated polystyrene resin-supported tungsten oxide. Three types of materials, including pristine polystyrene (PS), pristine polystyrene-supported tungsten oxide (PSWO), and sulfonated polystyrene-supported tungsten oxide (SO_3-PSWO), are synthesized and subjected to preliminary screening.

2.3 Characterization

Scanning electron microscopy (SEM) (TESCAN MAIA3 Triglav) is used to investigate the surface morphology, and energy-dispersive X-ray spectroscopy coupled with SEM is used to assess the loading of WO_3 in different host materials. An X-ray diffractometer (XRD) (EQUINOX 3000) with Cu K_α ($\lambda = 1.5408$ Å), step size 0.05°, and scan range between 10–80°, is used to study the structural characteristics. The thermal stability of the material is evaluated through thermogravimetric analysis (METLER TOLEDO GA/SDTA851) (TGA). C, H, N, and S elemental concentrations are determined using the elemental analyzer EA2 (ThermoFlash 2000, Italy). The amount of metal ions in adsorption studies is measured using an inductively coupled plasma-optical emission (ICP-OES) spectrometer (Thermo Scientific iCAP 6000).

2.4 Adsorption experiment

A 1000 mg L^{-1} stock solution is prepared by dissolving $PbCl_2$ in 250 mL of DI water. This stock solution is diluted as required for the adsorption experiments. For the batch adsorption study, 100 mg L^{-1} of Pb^{2+} solution containing 0.05 g of adsorbent (SO_3-PSWO) is used. The mixture is agitated at 250 rpm for 4 hours using a mechanical shaker to ensure sorption equilibrium. After centrifugation and filtration, concentrations of Pb^{2+} from the supernatant are determined by ICP-OES.

Adsorption capacity (mg g^{-1}) and removal efficiency (%) of prepared adsorbents are calculated using eqn (1) and (2), respectively.

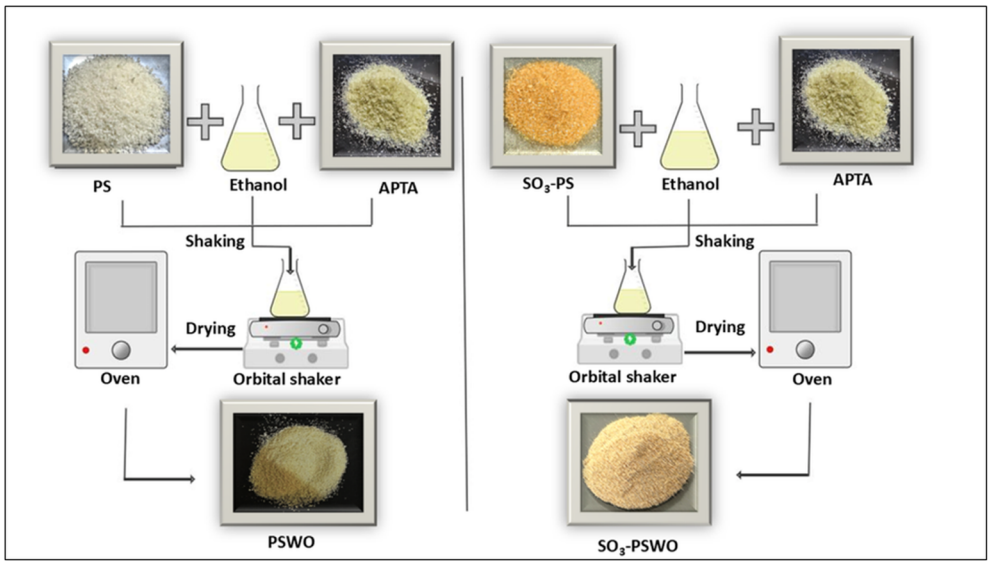

Fig. 3 Schematic illustration of the synthesis process of pristine polystyrene-supported tungsten oxide and sulfonated polystyrene-supported tungsten oxide.

$$\text{Adsorption capacity } (\text{mg g}^{-1}) = \frac{C_0 - C_e}{m} \times V \quad (1)$$

$$\text{Removal } (\%) = \frac{C_0 - C_e}{C_0} \times 100 \quad (2)$$

In eqn (1) and (2). C_0, C_e, m, and V are the initial and equilibrium concentrations (mg L^{-1}), the mass of the adsorbent taken in grams, and the volume of adsorbate in liters, respectively.

To evaluate the adsorption characteristics of Pb^{2+} ions under different conditions, experiments are conducted to study key parameters like pH, adsorbent dosage, contact time, initial metal ion concentration, temperature, and coexisting competing ions.

2.4.1 Optimization of pH. To find the maximum Pb^{2+} removal, three different adsorbents, *i.e.*, PS, PSWO, and SO_3-PSWO, are investigated at pH values ranging from 1 and 5.5. For this series of experiments, 0.05 g of each adsorbent in 100 mL of 100 mg L^{-1} of Pb^{2+} solution is shaken for 1 hour at 25 °C using a mechanical shaker set at 250 rpm. The pH adjustment is done using 0.1 M HNO_3 and NaOH solution.

2.4.2 Adsorption kinetic studies. To comprehend the adsorbent's kinetic performance, the pseudo-first-order (PFO) and pseudo-second-order (PSO) kinetic models are employed. Where, PFO and PSO rate constants for adsorption are represented in eqn (3) and (4) by k_1 (min^{-1}) and k_2 (mg g^{-1} min^{-1}), respectively. The q_e and q_t are adsorption capacity (mg g^{-1}) at equilibrium and at any time (t), respectively.

$$\ln(q_e - q_t) = \ln(q_e) - k_1 t \quad (3)$$

$$\frac{t}{q_t} = \frac{1}{k_2 q_e^2} + \frac{t}{q_e} \quad (4)$$

To investigate adsorption kinetics, 0.05 g of SO_3-PSWO is shaken with 100 mg L^{-1} Pb^{2+} solution on a mechanical shaker for 4 hours. Samples are collected at intervals of 5, 10, 20, 30, 45, 60, 120, 180, and 240 minutes, filtered using Whatman grade 42 filter paper having a pore size of 2.5 μm, and analyzed for Pb^{2+} concentrations.

2.4.3 Adsorption isotherms. The Langmuir and Freundlich isotherms are used to predict the maximum loading and mechanism of the adsorption process, and are written mathematically in eqn (5) and (6), respectively. Where, q_e, C_e, q_{max}, and K_L denote the adsorption capacity (mg g^{-1}), the concentration of adsorbate at equilibrium (mg L^{-1}), the maximum adsorption capacity of adsorbent, and the Langmuir constant, respectively. In the Freundlich isotherm equation, K_F, q_e, and n indicate the Freundlich isotherm constant, adsorption capacity, and heterogeneity factor, respectively.

$$\frac{C_e}{q_e} = \frac{1}{K_L q_{max}} + \frac{C_e}{q_{max}} \quad (5)$$

$$\ln(q_e) = \ln(K_F) - \frac{1}{n} \ln(C_e) \quad (6)$$

Langmuir parameter, R_L, which is the separation factor, indicates the favorability of the adsorption process. The dimensionless parameter R_L can be determined by the given eqn (7). The R_L value between 0 to 1 indicates the favorable nature, whereas, the corresponding value greater than 1 suggests the unfavorable nature of the adsorption process.[39]

$$R_L = \frac{1}{[1 + (K_L \times C_0)]} \quad (7)$$

To study the effect of initial metal ion concentration, Pb^{2+} solutions with 25, 50, 100, 150, and 200 mg L^{-1} concentrations are prepared. At each of these concentrations, 0.05 g of adsorbent is added, and the mixture is shaken for 1 hour. Residual

Pb^{2+} concentration is measured to evaluate adsorption capacity at varying initial concentrations.

The suitability of sorption isotherm models was assessed using the chi-square (χ^2) test and the linear regression coefficient (R^2). The chi-square test quantifies the discrepancies between experimental and model-predicted data by calculating the sum of squared errors, normalized by the model-derived values. The closely matched calculated adsorption capacity (q_{cal}) and the experimental adsorption capacity (q_{exp}) lead to the χ^2 value approaching zero, indicating a better fit. Conversely, larger differences between q_{cal} and q_{exp} result in higher χ^2 values. The mathematical expression for the χ^2 test is provided below for clarity.[40]

$$\chi^2 = \sum_{i=0}^{n} \frac{(q_{exp} - q_{cal})^2}{q_{cal}} \quad (8)$$

2.4.4 Thermodynamic studies. The Van't Hoff equation (eqn (9)) is used to analyze the thermodynamic characteristics of the adsorption process such as the standard enthalpy change ($\Delta H°$) and standard entropy change ($\Delta S°$).[41] The standard Gibbs free energy change ($\Delta G°$) at different temperatures is determined using (eqn (10)). Here, R is a general gas constant having a value of 8.314 J K^{-1} mol^{-1}, and ΔS and ΔH are calculated by plotting $\ln(k_c)$ *versus* $1/T$.

$$\ln(k_c) = \frac{\Delta S}{R} - \frac{\Delta H}{RT} \quad (9)$$

$$\Delta G = \Delta H - T\Delta S \quad (10)$$

The effect of temperature on Pb^{2+} adsorption is also studied at 298, 313, 323, and 333 K.

2.5 Statistical analysis

All experiments are conducted in triplicate, and the mean values with standard deviations are calculated to evaluate pH, adsorbent dosage, kinetics, and adsorption isotherms. Experimental adsorption data is analyzed by employing various isotherm and kinetic models using both linear and non-linear regression techniques.

3. Results and discussion

3.1 Morphology and phase characterization

SEM analysis is conducted to observe the morphology of polystyrene (PS), WO_3-incorporated PS (PSWO), and WO_3-incorporated sulfonated PS (SO_3-PSWO) adsorbents. Fig. 4(a–e) reveals a spherical bead-like morphology with surface variations in all the samples. For further clarity, digital photographs of PS, PSWO, SO_3-PS, and SO_3-PSWO are also included in the ESI as shown in Fig. S1(a–d).† This is a typical morphology of PS beads synthesized *via* suspension polymerization, where monomer droplets polymerize into stabilized beads due to agitation and surfactants.[42]

The surface of PS, *i.e.*, a pristine base polymer, is smooth (Fig. 4a), without the addition of WO_3 and functionalization, whereas the surface of PSWO is slightly rough (Fig. 4b and c), indicating the incorporation of WO_3 in it. The morphology of PSWO is similar to the PS-DVB/Fe_3O_4 core–shell beads synthesized elsewhere,[43] where beads exhibit a rough surface besides some pores and cavities after the Fe_3O_4 incorporation. This suggests that PS changes its structure because of the addition of WO_3, leading to increased surface irregularities and enhancing overall roughness. The EDS data of PSWO present in Fig. 4c (inset), indicates the W concentration of 3.1 wt%.

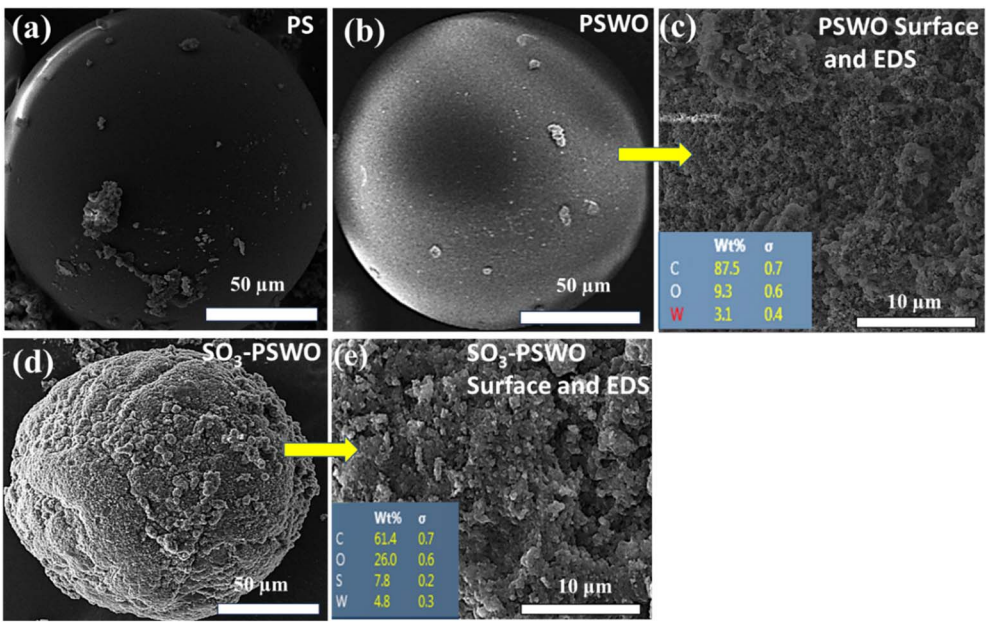

Fig. 4 SEM images of (a) PS and (b) PSWO, (c) the surface of PSWO bead along with its EDS spectrum, and (d and e) the SEM images of SO_3-PSWO at low and higher magnifications along with EDS data, respectively.

In the case of SO_3-PSWO (Fig. 4d and e), a more pronounced change in the surface morphology of beads can be observed. The significant change in surface roughness can be traced back to sulfonated PS, which is the base material of SO_3-PSWO. A similar morphology is reported by Martin *et al.*,[44] where the micrographs of the sulfonated resins show particles (P2S) with a spherical shape having irregular surfaces due to sulfuric acid treatment. This surface roughness originates from sulfonation due to the chemical introduction of sulfonic acid groups, which disrupts the polymer structure and can lead to localized degradation. This results in unevenness and increased porosity, enhancing the overall surface roughness. The roughness of the SO_3-PSWO can facilitate the efficient incorporation of WO_3 in the SO_3-PS support. The elemental mapping results, shown in Fig. S2,† demonstrate a uniform distribution of tungsten oxide particles throughout the host matrix, further confirming the successful incorporation of tungsten oxide in SO_3-PSWO. The degree of incorporation of WO_3 in SO_3-PSWO is comparatively higher, *i.e.* 4.8 wt% (Fig. 4e), compared with PSWO, which has 3.1 wt% W (Fig. 4c).[9]

XRD patterns of PS, PSWO, SO_3-PS, and SO_3-PSWO are shown in Fig. 5. In Fig. 5, PS exhibits a broad hump between at low 2θ values ranging from 10 to 30° indicating its amorphous nature without a regular and repeating pattern, likely because of the random distribution of monomers, *i.e.* styrene and divinylbenzene, during polymerization and uneven cross-linking of polymer chains through divinylbenzene.[45,46] The incorporation of WO_3 into PS (*i.e.* PSWO) shows two broad humps with no discernible peaks in the XRD pattern, indicating that the PSWO is still amorphous. This suggests that besides PS, WO_3 incorporated into PS reacted at 100 °C is also amorphous, meaning that the PS surface does not support the growth of crystalline WO_3. This is similar to the other studies where WO_3 grown on FTO substrate at low process temperature shows the amorphous nature.[47] The sulfonation typically involves introducing sulfonic acid ($-SO_3H$) groups onto the PS backbone, a treatment that generally further disrupts the regularity within the polymer introduced by the SO_3H groups and breaks the symmetry of the polymer chains.[48] This is why the SO_3-PS shows an even broader hump in the XRD pattern. Interestingly, when WO_3 is grown into SO_3-PS, its crystallinity increases, which is indicated by the appearance of distinct peaks in its XRD pattern. XRD peaks do not belong to any single phase; rather, SO_3-PSWO seems to be a mixture of two phases. The diffraction peak at the 2θ value of 16.5° corresponds to the (102) plane of monoclinic $W_{17}O_{47}$ with the PDF card no. 00-044-0396 with space group *P2/m*. Other peaks at 2θ values of 25.6, 35.0, 49.7, and 52.8° arise from (230), (231), (441), and (460) planes, respectively, with W_3O_8 orthorhombic crystal system with the PDF card no. 01-081-2263 having space group *Pbam*. These sharp and distinct peaks confirm that the synthesized WO_3 is crystalline. Typically, WO_3 is initially produced in an amorphous form at low temperatures, with crystallinity developing at temperatures of ≥400 °C.[49] This suggests that the SO_3H groups on PS may have promoted the crystallization of WO_3 from APTA, even at lower temperatures.

3.2 Thermal stability and structural analysis

The TGA analysis of PS, PSWO, and SO_3-PSWO (Fig. 6) reveals distinct thermal behaviors influenced by the sulfonic acid groups and tungsten oxide. The initial weight loss (5–6 wt%) in PS up to 200 °C is attributed to the evaporation of physically or surface-absorbed water.[50,51] In PSWO and SO_3-PSWO, a 21.7 wt% weight loss is linked to the elimination of physisorbed and chemisorbed structural water within the resin, as noted by Suleiman *et al.* (2007).[52] Between 200–350 °C, a major weight loss occurs, with SO_3-PSWO losing 69.61% and PSWO 78.6 wt%, primarily due to polymer backbone degradation. The presence of SO_3H in SO_3-PSWO promotes earlier decomposition. Tungsten oxide slightly enhances thermal stability, as evidenced by increased residue content in SO_3-PSWO compared to PSWO. In contrast, PS exhibits 85.18% weight loss between 250–500 °C, corresponding to polymer chain decomposition, leaving almost no residue beyond 550 °C, consistent with polystyrene's organic nature.[53]

The CHNS elemental composition of samples is determined by the CHNS elemental analyzer and is summarized in Table 1. CHNS analysis reveals that both PS and PSWO are rich in carbon

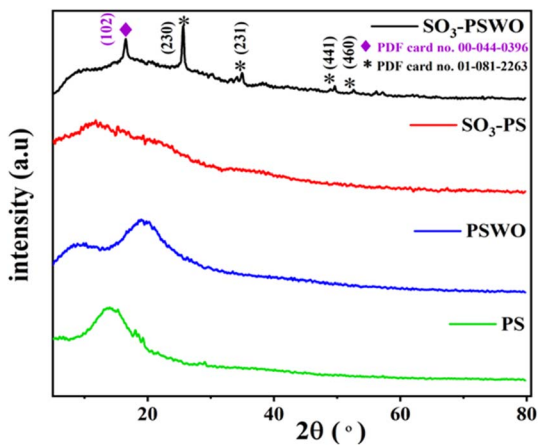

Fig. 5 XRD patterns of PS, PSWO, SO_3-PS, and SO_3-PSWO.

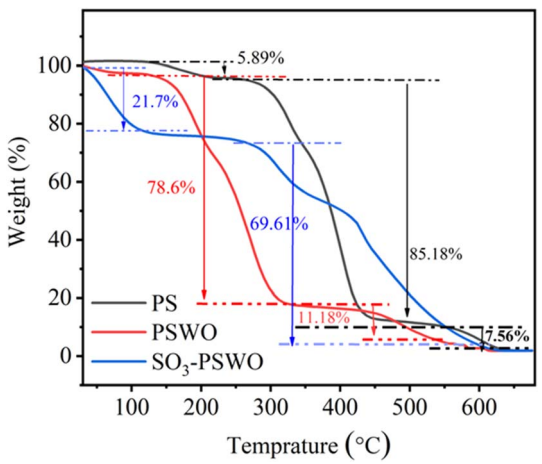

Fig. 6 Thermal stability analysis of PS, PSWO, and SO_3-PSWO.

Table 1 A summary of C, H, and S concentrations in prepared samples

Sample ID	C (wt%)	H (wt%)	S (wt%)
PS	85.0	7.0	ND
PSWO	85.9	7.3	ND
SO_3-PS	35.7	5.8	0.33
SO_3-PSWO	338.4	5.6	0.33

(C), with negligible changes in C and hydrogen (H) content after WO_3 incorporation. However, in SO_3-PSWO, a significant reduction in C content and the presence of 0.33 wt% of sulfur (S) confirm the successful sulfonation of PS beads before WO_3 loading. This marked decrease (over 50%) in C content in SO_3-PS and SO_3-PSWO is expected due to the introduction of sulfur groups and the heavy atomic mass of tungsten. Graphical representations of C, H, and S content across all samples are shown in Fig. S3.† The hydrogen concentration in sulfonated PS (5.8%) is slightly higher than in SO_3-PSWO (5.6%), suggesting that WO_3 primarily integrates with sulfonated PS through SO_3H functional groups.

Interestingly, a slight increase in C content is observed in both PSWO and SO_3-PSWO after WO_3 incorporation using acetyl peroxotungstic acid compared to their counterparts' PS and SO_3-PS. This increase is more pronounced in sulfonated PS, likely due to residual acetyl groups retained in the polymer matrix. The higher polarity of sulfonated PS, attributed to SO_3H groups, may facilitate stronger interactions with the acetyl species, leading to its greater retention.

3.3 Absorption studies

3.3.1 Effect of pH. The adsorbent's surface charge and the adsorbate's chemistry are both strongly influenced by pH.[54] For pH adsorption studies, three sorbents, PS (pristine), PSWO (pristine with WO_3), and SO_3-PSWO (pristine with WO_3 and SO_3H), are mainly focused.

In Fig. 7a, PS exhibits minimal change in adsorption across the tested pH range, with a slight increase at pH 4.5–5.5. In contrast, PSWO shows a significant increase in Pb^{2+} removal efficiency, rising from 8% at pH 1 to 89% at pH 5.5, attributed to the amorphous WO_3. However, its efficiency does not exceed 95%. SO_3-PSWO demonstrates superior adsorption across all pH values, achieving 98% removal at pH 3.5 and reaching 99.7% at pH 5.5. The study is conducted within a pH range of 1 to 5.5 to prevent Pb^{2+} precipitation at higher pH levels.[9] Above pH 5.5, interfering species such as $Pb(OH)^+$ and $Pb(OH)_2$ begin to form, resulting in weaker sorption or precipitation from the solution. Consequently, the pH is maintained at 5.5 throughout the upcoming experiments.

The higher removal efficiencies of PSWO and SO_3-PSWO at elevated pH levels can be attributed to reduced proton competition with Pb^{2+} for adsorption sites. Additionally, variations in the swelling behavior of polystyrene may contribute to this trend, as the polymer undergoes ionization-induced swelling at higher pH values. When acidic functional groups ionize above their pK_a, the resulting negative charges on the polymer chains increase electrostatic repulsion, causing expansion. Similar swelling behavior has been reported by Rizwan *et al.* (2017).[55] For kinetic and adsorption modeling studies, SO_3-PSWO is selected due to its highest removal efficiency at pH 5.5.

3.3.2 Effect of adsorbent dose. Conducting an adsorbent dose experiment is essential in adsorption studies to determine the impact of adsorbent concentration on removal efficiency and adsorption capacity. In this study, the effect of SO_3-PSWO dosage on Pb^{2+} removal is evaluated by varying the adsorbent concentration from 0.1 to 5 g L^{-1} while keeping all other experimental conditions constant.

As shown in Fig. 7b, the Pb^{2+} removal efficiency increases from 80.1% at 0.1 g L^{-1} to over 99% at 0.5 g L^{-1}. Beyond this dosage, up to 5 g L^{-1}, removal efficiency remains consistently above 99%. These findings suggest that 0.5 g L^{-1} is the optimal adsorbent dose, as a further increase in dosage does not significantly enhance removal efficiency and may make the process less cost-effective.

3.3.3 Adsorption kinetics and adsorption isotherms. To gain more insight into the sorption process, the rate of adsorption is determined by fitting the experimental data following different kinetic models. Fig. 8c shows that more than 90% of Pb^{2+} is removed by SO_3-PSWO in 10 minutes and adsorption reaches the equilibrium within 1 hour. This

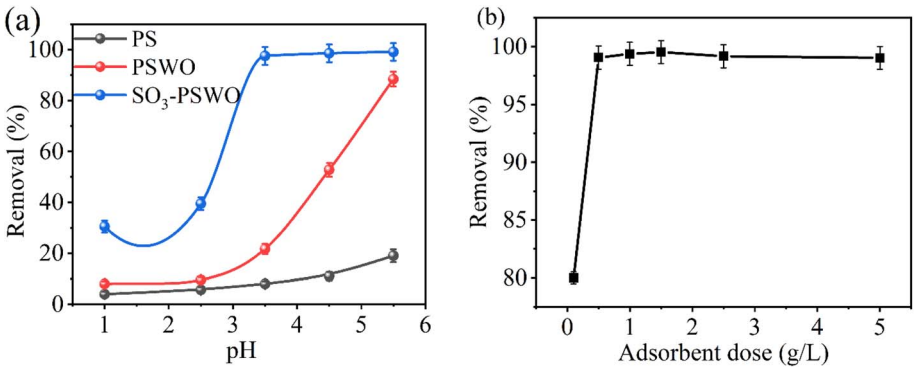

Fig. 7 (a) Effect of pH ranging from 1 to 5.5 on adsorption of Pb^{2+} onto PS, PSWO, and SO_3-PSWO and (b) effect of adsorbent dose in the range of 0.1 to 5 g L^{-1} on adsorption efficiency of the SO_3-PSWO (C_0 = 100 mg L^{-1}, S : L ratio = 0.5 g L^{-1}, contact time = 1 hour, shaking speed = 250 rpm).

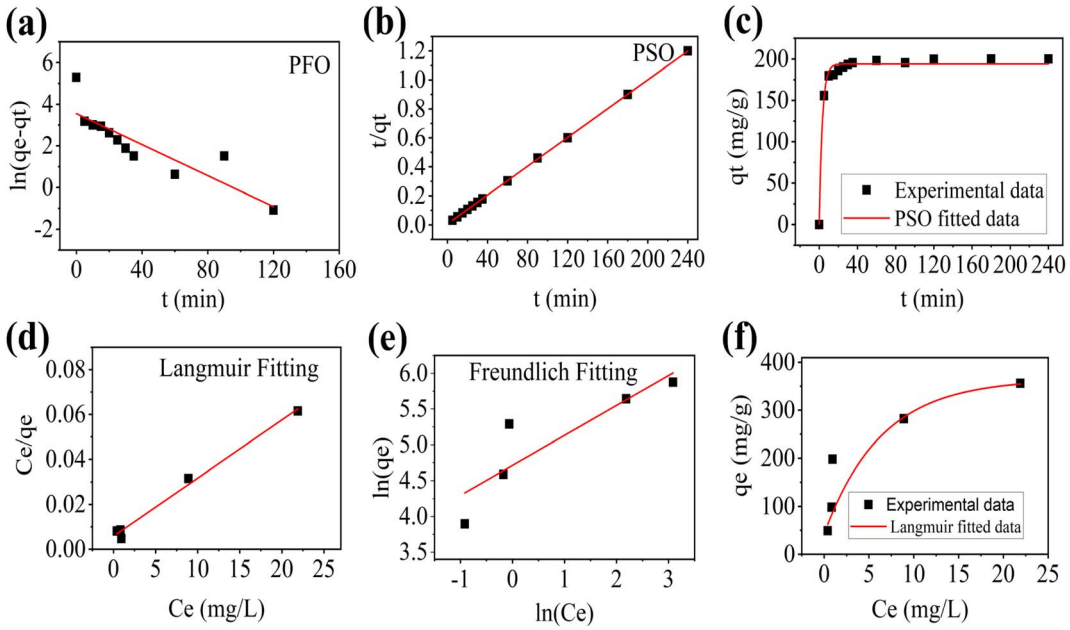

Fig. 8 Adsorption kinetics, (a) $\ln(q_e - q_t)$ *versus* t for PFO model fitting, (b) t/q_t *versus* t for PSO model fitting, and (c) q_t *versus* t data fitted with PSO model (contact time = 240 minutes, shaking speed = 250 rpm, C_0 = 100 mg L^{-1}, pH = 5.5, S : L ratio = 0.5 g L^{-1}). Adsorption isotherm models (d) Langmuir linear fitted model, (e) Freundlich linear fitted models, and (f) Langmuir curved fitted model of Pb^{2+} onto SO_3-PSWO.

Table 2 A summary of the comparison between PFO and PSO model parameters

Parameters	PFO	PSO
Experimental q_e (mg g^{-1})	200.0	200.0
Calculated q_e (mg g^{-1})	34.9	201.2
Rate constants (k_1 and k_2)	1.10×10^{-5} min^{-1}	0.0035 g mg^{-1} min^{-1}
R^2	0.7320	0.9999

indicates that the active sites on SO_3-PSWO are already saturated with Pb^{2+} ions, which is the cause of electrostatic repulsion for incoming Pb^{2+} ions.[56] To better understand the adsorption kinetics and determine the rate constants, the data is fitted to pseudo-first-order (PFO) and pseudo-second-order (PSO) models (eqn (3) and (4)). The linearized form of the PFO model (Fig. 8a) shows a poor correlation, with a regression coefficient (R^2) of 0.732, indicating that the PFO model does not adequately describe the adsorption kinetics. In contrast, the PSO model, plotted as t/q_t *versus* t in Fig. 8b, exhibits an excellent linear fit, with an R^2 value of 0.9999. The experimental and calculated q_e values for PSO (200.0 and 201.2 mg g^{-1}, respectively) are also in close agreement, as summarized in Table 2.

The good fitting of experimental data with the PSO model suggests that Pb^{2+} undergoes chemisorption on the SO_3-PSWO surface through electrostatic interaction between adsorbent surface functional groups (SO_3H) and Pb^{2+} ions.[57] The Pb^{2+} ions chemisorption on the SO_3-PSWO surface may occur through ion exchange or complexation reactions. In terms of adsorption, the chemisorption process is preferred over physisorption due to the strong adherence between the adsorbent and the adsorbate.

The concentration of metal ions, specifically Pb^{2+} in this study, significantly influences the adsorption. At lower Pb^{2+} concentrations, removal efficiency is typically high due to the abundance of available adsorption sites. However, as Pb^{2+} concentration increases, the removal efficiency declines. This reduction is primarily attributed to the finite number of adsorption sites on the adsorbent surface, which become saturated at higher metal ion concentrations. Additionally, a higher Pb^{2+} concentration enhances the driving force for adsorption, increasing the mass transfer of Pb^{2+} ions from the liquid phase and thereby raising the adsorption capacity.[58]

To evaluate the adsorption behavior, experimental isotherm data is obtained by varying Pb^{2+} concentrations from 25 to 200 mg L^{-1} and analyzing the data using the Freundlich and Langmuir isotherm models. Fig. 8d and e illustrate the fitting of the Langmuir and Freundlich models to the experimental data, while Fig. 8f presents the overlay of Langmuir-fitted data with experimental results. The Langmuir model plotted as C_e/q_e *versus* C_e (Fig. 8d), exhibits an excellent fit, with an R^2 value of 0.9903. In contrast, the Freundlich model is based on the linear fit of $\ln(q_e)$ and $\ln C_e$ results in a lower R^2 value of 0.7837. Furthermore, the χ^2 value for the Langmuir model (2.18) is significantly lower than that for the Freundlich model (5.19), further confirming that Langmuir provides a superior fit.

The better agreement of the experimental data with the Langmuir model suggests that Pb^{2+} adsorption onto SO_3-PSWO likely occurrs *via* chemisorption, involving monolayer coverage of metal binding sites. A summary of parameters obtained by fitting the experimental data following the adsorption isotherm models is provided in Table 3. Importantly, the Langmuir isotherm for SO_3-PSWO yields a maximum adsorption capacity

Table 3 A summary of different parameters determined from fitting experimental data of Pb^{2+} adsorption using SO_3-PSWO as an adsorbent following Langmuir and Freundlich isotherms

Type of isotherm	Parameter	Values
Langmuir	Q_{max} (mg g^{-1})	386.10
	K_L (L mg^{-1})	0.4442
	R_L	0.6508
	R^2	0.9903
	χ^2	2.18
Freundlich	K_F	111.41
	n	2.3889
	R^2	0.7837
	χ^2	5.19

(q_{max}) of 386.10 mg g^{-1}. Additionally, the Freundlich constant (n) of 2.39 and the dimensionless factor, R_L, of 0.65 from the Langmuir model indicate that the adsorption process is advantageous.[39]

3.3.4 Thermodynamics studies. The equilibrium constant (k_c) values for Pb^{2+} adsorption on SO_3-PSWO are determined using Van't Hoff's equation (eqn (9)) at different temperatures ranging from 298 to 333 K. A plot showing the linear change in $\ln(k_c)$ against $1/T$ in Fig. 9, indicates that the adsorption effectiveness is higher at lower temperatures. Lower k_c values at higher temperatures arise from the weakening of the chemical interaction connecting Pb^{2+} with adsorption sites.[59]

Thermodynamic parameters, including the enthalpy change ($\Delta H°$) and entropy change ($\Delta S°$), are calculated using eqn (9), yielding values of −14.55 kJ mol^{-1} and −0.004 kJ mol^{-1} K^{-1}, respectively. The negative $\Delta H°$ confirms that the adsorption process is exothermic, meaning heat is released as Pb^{2+} ions bind to the SO_3-PSWO surface. This exothermic nature stabilizes the system, as Pb^{2+} adsorption leads to a lower energy state, making the process thermodynamically favorable.

Furthermore, a negative $\Delta S°$ value indicates a decrease in disorder, which means the reduction in entropy at the solid–liquid interface during the adsorption of Pb^{2+} ions. This shows that the system achieves greater order as Pb^{2+} ions transition from the solution to the adsorbent surface, likely due to the organized arrangement of ions and water molecules surrounding the adsorption site.[60] The adsorption process is most efficient at room temperature, where moderate thermal energy allows Pb^{2+} ions to interact with the adsorbent's active sites. At elevated temperatures, increased ion mobility disrupts adsorption equilibrium, reducing adsorption efficiency.

Using the determined $\Delta H°$ and $\Delta S°$ values at different temperatures, $\Delta G°$ is also calculated using the standard Gibbs free energy equation (eqn (10)), and the corresponding values are summarized in the Table 4. As the temperature is increased from 298 to 333 K, the value of $\Delta G°$ slightly increases from −13.22 to −13.07 kJ mol^{-1}. The overall negative value of $\Delta G°$ represents the spontaneity of the adsorption process,[56] and its gradual increase from −13.22 to −13.07 kJ mol^{-1} indicates that the adsorption process becomes increasingly less favorable as the temperature increases.

3.3.5 Effect of counter ions. Competing ions can affect adsorption efficiency by influencing the availability of active binding sites on the adsorbent and altering the adsorption process through electrostatic interactions, charge density, competition for active sites, hydration effects, *etc.* Therefore, SO_3-PSWO is checked for its removal efficiency of Pb^{2+} in the presence of two divalent cations, including Ca^{2+} and Mg^{2+}, and two monovalent cations, including Na^+ and K^+.

The impact of coexisting ions, such as Mg^{2+}, Ca^{2+}, Na^+, and K^+, on Pb^{2+} adsorption is also evaluated. Equimolar concentrations of Pb^{2+} (100 mg L^{-1}) and Mg^{2+} or Ca^{2+} are prepared, and 0.05 g adsorbent is added to 100 mL of the mixed solution, which is shaken for 1 hour. The residual concentration of Pb^{2+}, Ca^{2+}, Mg^{2+}, Na^+, and K^+ is analyzed to assess the preferential adsorption of SO_3-PSWO for Pb^{2+} in the presence of these competing ions.

Fig. 10 exhibited an excellent removal (99.7%) of Pb^{2+}. Notably, the presence of competing cations did not affect the performance of SO_3-PSWO, highlighting its high adsorption capacity for Pb^{2+} ions. It is also worth noting that SO_3-PSWO shows almost the same removal for divalent and monovalent metal cations (≥80%). The adsorption process likely involves both electrostatic interactions and ion exchange, where SO_3H groups facilitate the uptake of cations irrespective of their charge. This broad affinity may contribute to the observed similar removal rates for monovalent and divalent cations. Moreover, the presence of SO_3H groups on the polymer matrix

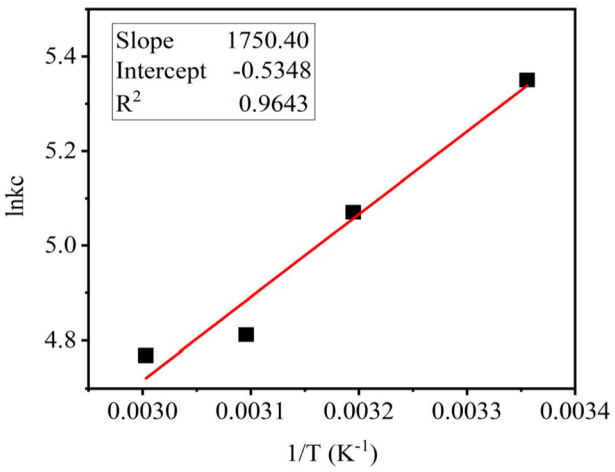

Fig. 9 $\ln(k_c)$ *versus* $1/T$ for Pb^{2+} adsorption onto SO_3-PSWO to determine the change in enthalpy and entropy (C_0 = 100 mg L^{-1}, S : L ratio 0.5 g L^{-1}, pH = 5.5, contact time = 1 hour).

Table 4 Thermodynamics data of Pb^{2+} adsorption on SO_3-PSWO in the temperature range of 303 to 333 K

$\Delta H°$ (kJ mol^{-1})	$\Delta S°$ (kJ mol^{-1} K^{-1})	Temperature (K)	$\Delta G°$ (kJ mol^{-1})
−14.55	−0.004	298	−13.22
		313	−13.16
		323	−13.11
		333	−13.07

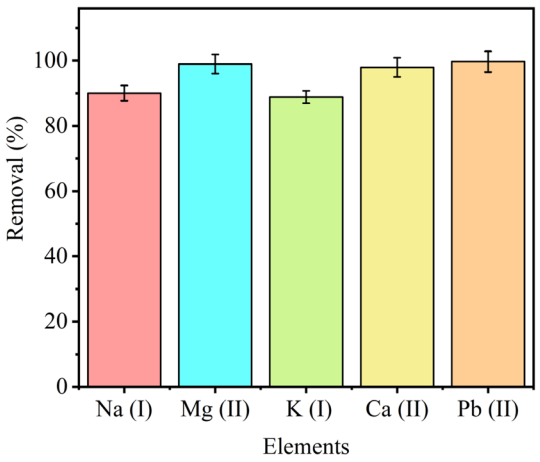

Fig. 10 Effect of interfering ions on Pb^{2+} adsorption by SO_3-PSWO (C_0 = 100 mg L^{-1}, S : L ratio 0.5 g L^{-1}, pH = 5.5, contact time = 1 hour).

can interact with various cations without a strict preference for divalent ions like Pb^{2+}. This suggests that the material's adsorption behavior is influenced by both charge and steric effects rather than a rigid selectivity pattern.

3.3.6 Regeneration and reusability. Reusability is a crucial factor in water treatment processes as it helps reduce costs and minimize secondary waste generation.[61] To evaluate this parameter, 0.05 g of used SO_3-PSWO is regenerated using a 0.1 M HNO_3 solution, followed by thorough washing with deionized water to remove desorbed contaminants and residual acid. The regenerated SO_3-PSWO is then tested for Pb^{2+} removal under identical conditions across four consecutive cycles.

The results shown in Fig. 11, indicate a slight decrease in Pb^{2+} removal efficiency after the the third cycle. However, at a concentration of 100 mg L^{-1}, the removal efficiency slightly decreased up to 7% after four cycles.

The ability to maintain high removal efficiency over multiple regeneration cycles underscores the adsorbent's durability and cost-effectiveness. Additionally, its reusability reduces the frequency of adsorbent replacement and minimizes secondary waste generation, making SO_3-PSWO an environmentally friendly and economically viable option for practical water treatment applications.

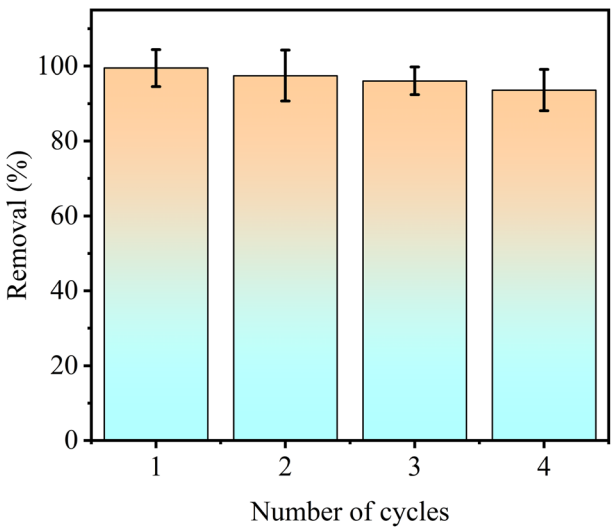

Fig. 11 Regeneration and reusability of SO_3-PSWO for Pb^{2+} removal.

A comparison of pre-adsorption and post-adsorption characterization using FTIR and SEM is performed, and results are reported in Fig. S4 and S5,† respectively. Successful Pb^{2+} adsorption by SO_3-PSWO is indicated by FTIR by decreasing the intensity of W–O–O, W–O, and W–OH and W=O bands, as shown in Fig. S4b.†

The SEM image of SO_3-PSWO pre-adsorption (Fig. S5a†) shows a smooth surface, while the SEM image in post adsorption of Pb^{2+} (Fig. S5b†) reveals observable changes on the surface. These alterations are probably due to Pb^{2+} ion adsorption by SO_3-PSWO surface or inside pores of the matrix.

3.3.7 Comparison with other adsorbents. The adsorption capacity of SO_3-PSWO for Pb^{2+} removal surpasses various functionalized polymeric materials, commercially available tungsten oxide, and MoS_2, as detailed in Table 5. With a maximum adsorption capacity of 386.1 mg g^{-1}, SO_3-PSWO outperforms all listed alternatives, establishing itself as a superior candidate for Pb^{2+} ion removal from aqueous solutions.

This exceptional performance can be attributed to its dual adsorption mechanism, combining electrostatic attraction facilitated by SO_3H groups with strong chemical bonding offered by tungsten oxide. The synergistic interaction between these components enhances the adsorption capacity and ensures rapid uptake kinetics, making SO_3-PSWO highly effective for water treatment applications.

The high adsorption capacity of SO_3-PSWO positions it as a promising material for practical environmental remediation, especially in scenarios involving heavy metal contamination. Its ability to outperform traditional adsorbents demonstrates its potential for large-scale deployment in water purification systems, aligning with the growing demand for efficient, cost-effective, and sustainable solutions to mitigate water pollution.

3.4 Possible adsorption mechanism

The SO_3-PSWO composite, comprising tungsten oxide and sulfonated polystyrene resin, demonstrates higher efficiency in removing Pb^{2+} ions from aqueous solutions. The adsorption mechanism leverages multiple binding sites provided by tungsten oxide and sulfonate groups, employing electrostatic attraction and chemical binding for enhanced performance. The SO_3H group, with its negative charge, attracts Pb^{2+} ions electrostatically, even in the presence of competing ions.[9]

Additionally, tungsten oxide offers specific surface sites for Pb^{2+} ions, forming stable coordination complexes. This dual mechanism ensures efficient capture: Pb^{2+} ions are initially bound to the SO_3H groups through electrostatic interactions, followed by tungsten oxide forming strong chemical bonds, leading to stable surface complexes. The strong affinity of tungsten oxide for Pb^{2+} ions supports a monolayer adsorption behavior consistent with the Langmuir model. Even without the SO_3H group, tungsten oxide exhibits significant adsorption

Table 5 Comparison of adsorption capacities of different adsorbents for removal of Pb^{2+}

Adsorbents	Adsorption capacity (mg g^{-1})	References
Chelating resin functionalized with dithiooxamide	24.3	62
CFA/GO/WO_3NRs	41.5	34
Poly(MMA–MAGA) functionalized with methacryloylamidoglutamic acid groups	65.2	63
Poly(styrene-*co*-divinylbenzene)amine	73.0	64
Polyhedral oligomeric silsesquioxanes (POSS) incorporated with Fe_3O_4	90.9	65
EGTA-modified chitosan	101.4	66
Polyacrylamide-hydrated ferric oxide hybrid material	211.4	67
NZP (hydrated Zr(IV) oxide inside a commercial cation exchange resin D-001 nanocomposite)	319.4	9
Commercially available tungsten trioxide (WO_3)	324.0	32
MoS_2	366.0	68
SO_3-PSWO	386.1	This study

capability, as evidenced by PSWO, which achieves 89% Pb^{2+} removal. The synergetic effect of SO_3H groups and tungsten oxide enhances both the efficiency and rate of Pb^{2+} ion removal, showcasing the material's potential for effective heavy metal remediation.[69]

4. Conclusion

This study successfully synthesized sulfonated polystyrene resin-supported tungsten oxide (SO_3-PSWO) and investigated its efficiency in removing Pb^{2+} ions from aqueous solutions. A comparative analysis with pristine polystyrene resin-supported tungsten oxide demonstrated the superior performance of SO_3-PSWO, attributed to the higher loading of tungsten oxide facilitated by the sulfonic acid groups. XRD analysis confirmed the crystalline nature of tungsten oxide on SO_3-PSWO, in contrast to its amorphous form on pristine polystyrene.

Comprehensive characterization using SEM, XRD, TGA, CHNS analyzer, and ICP-OES revealed critical insights into the material's morphology, structural properties, thermal stability, and elemental compositions. Adsorption performance is evaluated across various parameters, including pH, adsorbent dosage, contact time, Pb^{2+} concentration, temperature, and competing ions. SO_3-PSWO demonstrated remarkable removal efficiency, achieving near-complete Pb^{2+} removal within an hour in the pH range of 3.5–5.5. The maximum adsorption capacity reached 386 mg g^{-1}, aligning well with the Langmuir isotherm model, while kinetic studies indicated a chemisorption-driven pseudo-second-order process.

Thermodynamic analysis revealed the adsorption process to be exothermic and spontaneous. The combined effects of sulfonic acid groups and tungsten oxide might have contributed to the high adsorption capacity, making SO_3-PSWO a promising material for removing Pb^{2+} ions from industrial effluents. These findings emphasize its potential as a cost-effective and efficient solution for mitigating heavy metal contamination in water treatment applications.

Data availability

Data will be available on request.

Conflicts of interest

There are no conflicts to declare.

References

1 T. Zhang, P. Li, S. Ding and X. Wang, *J. Hazard. Mater.*, 2022, **424**, 127742.
2 D. Purkayastha, U. Mishra and S. Biswas, *J. Water Process Eng.*, 2014, **2**, 105–128.
3 H. Alidadi, S. B. Tavakoly Sany, B. Zarif Garaati Oftadeh, T. Mohamad, H. Shamszade and M. Fakhari, *Environ. Health Prev. Med.*, 2019, **24**, 1–17.
4 M. Parmar and L. S. Thakur, *Int. J. Plant, Anim. Environ. Sci.*, 2013, **3**, 143–157.
5 S. Ray and M. K. Ray, *Al Ameen J. Med. Sci.*, 2009, **2**, 57–63.
6 K. K. Das, R. C. Reddy, I. B. Bagoji, S. Das, S. Bagali, L. Mullur, J. P. Khodnapur and M. Biradar, *J. Basic Clin. Physiol. Pharmacol.*, 2019, **30**, 141–152.
7 K. Vikrant and K.-H. Kim, *Chem. Eng. J.*, 2019, **358**, 264–282.
8 F. Fernandez-Luqueno, F. Lopez-Valdez, P. Gamero-Melo, S. Luna-Suarez, E. N. Aguilera-Gonzalez, A. I. Martínez, M. García-Guillermo, G. Hernandez-Martinez, R. Herrera-Mendoza and M. A. Álvarez-Garza, *J. Environ. Sci. Technol.*, 2013, **7**, 567–584.
9 M. Hua, Y. Jiang, B. Wu, B. Pan, X. Zhao and Q. Zhang, *ACS Appl. Mater. Interfaces*, 2013, **5**, 12135–12142.
10 M. Fida, P. Li, Y. Wang, S. K. Alam and A. Nsabimana, *Exposure Health*, 2023, **15**, 619–639.
11 S. Gunatilake, *Methods*, 2015, **1**, 14.
12 M. Rose, M. Baxter, N. Brereton and C. Baskaran, *Food Addit. Contam.*, 2010, **27**, 1380–1404.
13 M. Loghman-Adham, *Environ. Health Perspect.*, 1997, **105**, 928–939.
14 D. A. Gidlow, *Occup. Med.*, 2015, **65**, 348–356.
15 P. Froom, E. Kristal-Boneh, J. Benbassat, R. Ashkanazi and J. Ribak, *Clin. Chem.*, 1998, **44**, 1283–1288.
16 P. Mitra, S. Sharma, P. Purohit and P. Sharma, *Crit. Rev. Clin. Lab. Sci.*, 2017, **54**, 506–528.
17 J. Su, D. Ji, M. Lin, Y. Chen, Y. Sun, S. Huo, J. Zhu and B. Xi, *Resour., Conserv. Recycl.*, 2017, **117**, 294–303.

18 A. Xu, Y.-H. Wu, Z. Chen, G. Wu, Q. Wu, F. Ling, W. E. Huang and H.-Y. Hu, *Water Cycle*, 2020, **1**, 80–87.
19 S. Wan, X. Zhao, L. Lv, Q. Su, H. Gu, B. Pan, W. Zhang, Z. Lin and J. Luan, *Ind. Eng. Chem. Res.*, 2010, **49**, 7574–7579.
20 T. A. Kurniawan, G. Y. Chan, W.-H. Lo and S. Babel, *Chem. Eng. J.*, 2006, **118**, 83–98.
21 D. W. O'Connell, C. Birkinshaw and T. F. O'Dwyer, *Bioresour. Technol.*, 2008, **99**, 6709–6724.
22 F. Fu and Q. Wang, *J. Environ. Manage.*, 2011, **92**, 407–418.
23 H. Eccles, *Trends Biotechnol.*, 1999, **17**, 462–465.
24 Y. Sharma, U. S. Upadhyay and F. Gode, *J. Appl. Sci. Environ. Sanit.*, 2009, **4**, 21–24.
25 B. Pan, B. Pan, W. Zhang, L. Lv, Q. Zhang and S. Zheng, *Chem. Eng. J.*, 2009, **151**, 19–29.
26 G. Zhao, X. Wu, X. Tan and X. Wang, *Open Colloid Sci. J.*, 2010, **4**, 19–31.
27 M. Hua, Y. Jiang, B. Wu, B. Pan, X. Zhao and Q. Zhang, *ACS Appl. Mater. Interfaces*, 2013, **5**, 12135–12142.
28 H. Tabekh, M. H. Al Kurdi and Z. Ajji, *Polimeri*, 2015, **36**, 11–14.
29 Q. Zhang, Q. Du, M. Hua, T. Jiao, F. Gao and B. Pan, *Environ. Sci. Technol.*, 2013, **47**, 6536–6544.
30 P. Trivedi, L. Axe and T. A. Tyson, *Environ. Sci. Technol.*, 2001, **35**, 4515–4521.
31 Y. Wang, H. Huang, S. Duan, X. Liu, J. Sun, T. Hayat, A. Alsaedi and J. Li, *ACS Sustain. Chem. Eng.*, 2018, **6**, 2462–2473.
32 C. K. Perkins, T. M. Reed and A. W. Apblett, *RSC Adv.*, 2015, **5**, 68991–68997.
33 C. K. Perkins, T. M. Reed, Z. A. Brown and A. W. Apblett, *Environ. Sci.:Water Res. Technol.*, 2017, **3**, 429–432.
34 E. C. Umejuru, E. Prabakaran and K. Pillay, *ACS Omega*, 2021, **6**, 11155–11172.
35 A. A. Keller, H. Wang, D. Zhou, H. S. Lenihan, G. Cherr, B. J. Cardinale, R. Miller and Z. Ji, *Environ. Sci. Technol.*, 2010, **44**, 1962–1967.
36 V. Chandra, J. Park, Y. Chun, J. W. Lee, I.-C. Hwang and K. S. Kim, *ACS Nano*, 2010, **4**, 3979–3986.
37 S. Sarkar, A. K. SenGupta and P. Prakash, *Environ. Sci. Technol.*, 2010, **44**, 1161–1166.
38 Q. Zhang, B. Pan, B. Pan, W. Zhang, K. Jia and Q. Zhang, *Environ. Sci. Technol.*, 2008, **42**, 4140–4145.
39 M. B. Desta, *Environ. Sci. Technol.*, 2013, **2013**, 375830.
40 S. Z.-e.-H. Ejaz, S. Iqbal, S. Shahida, S. M. Husnain and M. Saifullah, *New J. Chem.*, 2023, **47**, 443–452.
41 C. Han, L. Yang, H. Yu, Y. Luo and X. Shan, *Environ. Sci. Pollut. Res.*, 2020, **27**, 2455–2463.
42 H. Yuan, G. Kalfas and W. Ray, *J. Macromol. Sci., Part C*, 1991, **31**, 215–299.
43 M. A. Ali, M. F. Mubarak, M. Keshawy, M. A. Zayed and M. Ataalla, *Alexandria Eng. J.*, 2022, **61**, 1335–1352.
44 C. Martin, L. Ramirez and J. Cuellar, *Surf. Coat. Technol.*, 2003, **165**, 58–64.
45 N. Manikandan, *Int. J. Recent Innovation Trends Comput. Commun.*, 2014, **2**, 1148–1151.
46 X. Fu and S. Qutubuddin, *Mater. Lett.*, 2000, **42**, 12–15.
47 J. Han, K.-w. Ko, S. Sarwar, M.-s. Lee, S. Park, S. Hong and C.-h. Han, *Electrochim. Acta*, 2018, **278**, 396–404.
48 A. Al-Sabagh, Y. Moustafa, A. Hamdy, H. Killa, R. Ghanem and R. Morsi, *Egypt. J. Pet.*, 2018, **27**, 403–413.
49 C. Santato, M. Odziemkowski, M. Ulmann and J. Augustynski, *J. Am. Chem. Soc.*, 2001, **123**, 10639–10649.
50 T. Faravelli, M. Pinciroli, F. Pisano, G. Bozzano, M. Dente and E. Ranzi, *J. Anal. Appl. Pyrolysis*, 2001, **60**, 103–121.
51 Q. Zheng and R. Morgan, *J. Compos. Mater.*, 1993, **27**, 1465–1478.
52 D. Suleiman, E. Napadensky, J. M. Sloan and D. M. Crawford, *Thermochim. Acta*, 2007, **460**, 35–40.
53 B. N. Jang and C. A. Wilkie, *Polym. J.*, 2005, **46**, 2933–2942.
54 R. Karthik and S. Meenakshi, *J. Water Process Eng.*, 2014, **1**, 37–45.
55 M. Rizwan, R. Yahya, A. Hassan, M. Yar, A. D. Azzahari, V. Selvanathan, F. Sonsudin and C. N. Abouloula, *Polym. J.*, 2017, **9**, 137.
56 K. Mumtaz, S. Iqbal, S. Shahida, M. A. Shafique, M. Wasim and B. Ahmad, *Microporous Mesoporous Mater.*, 2021, **326**, 111361.
57 W. Cai, M. Gu, W. Jin and J. Zhou, *J. Alloys Compd.*, 2019, **777**, 1304–1312.
58 W. Zhang, S. Zhang, J. Wang, M. Wang, Q. He, J. Song, H. Wang and J. Zhou, *Chemosphere*, 2018, **203**, 188–198.
59 L. Tian, G. Xie, R.-x. Li, X.-h. Yu and Y.-q. Hou, *Desalin. Water Treat.*, 2011, **36**, 334–343.
60 O. O. Rukayat, M. F. Usman, O. M. Elizabeth, O. O. Abosede and I. U. Faith, *S. Afr. J. Chem. Eng.*, 2021, **37**, 74–80.
61 M. A. R. Anjum, S. Iqbal, Z. Toba, S. Javaid, A. Jamal, M. A. Shafique and M. S. Ullah, *New J. Chem.*, 2023, **47**, 18260–18271.
62 S. Dutta and A. Das, *J. Appl. Polym. Sci.*, 2007, **103**, 2281–2285.
63 A. Denizli, N. Sanli, B. Garipcan, S. Patir and G. Alsancak, *Ind. Eng. Chem. Res.*, 2004, **43**, 6095–6101.
64 B. L. Rivas, S. A. Pooley, H. A. Maturana and S. Villegas, *J. Appl. Polym. Sci.*, 2001, **80**, 2123–2127.
65 A. Akbari, N. Arsalani, B. Eftekhari-Sis, M. Amini, G. Gohari and E. Jabbari, *Front. Chem. Sci. Eng.*, 2019, **13**, 563–573.
66 F. Zhao, E. Repo, D. Yin and M. E. Sillanpää, *J. Colloid Interface Sci.*, 2013, **409**, 174–182.
67 G. Manju, K. A. Krishnan, V. Vinod and T. Anirudhan, *J. Hazard. Mater.*, 2002, **91**, 221–238.
68 C. Liu, S. Zeng, B. Yang, F. Jia and S. Song, *J. Mol. Liq.*, 2019, **296**, 111987.
69 Y. Wang, H. Huang, S. Duan, X. Liu, J. Sun, T. Hayat, A. Alsaedi and J. Li, *ACS Sustain. Chem. Eng.*, 2018, **6**, 2462–2473.